

Supplemental Experimental Procedures

Patients and healthy control samples. All human samples were obtained after informed consent following the guidelines of the Institutional Review Board of the Institute of Hematology and Blood Disease Hospital, Tianjin, China. Peripheral blood (PB) samples were obtained from healthy donors and patients with acute B-lymphocytic leukemia (B-ALL). PB low-density mononuclear cells (MNCs) were purified using Ficoll-Hypaque. A CD19⁺ cell population was isolated using a magnetic activated cell sorting CD19⁺ Isolation Kit (Miltenyi Biotec).

Generation and maintenance of *Tet1/2* double-mutant (*DKO*) Mice. *Tet1/2 DKO* mice were generated as previously reported (Dawlaty et al., 2013). Briefly, *Tet1*^{-/-} and *Tet2*^{-/-} mice (Dawlaty et al., 2011; Li et al., 2011) were crossed to obtain *Tet1*^{+/-};*Tet2*^{+/-} animals, which were further intercrossed to produce experimental animals including *DKO*, *Tet1*^{-/-}, *Tet2*^{-/-}, *Tet1*^{+/-};*Tet2*^{-/-}, and WT mice. Quantitative RT-PCR analysis showed that the *Tet1* mRNA expression was not detectable in the *Tet1*^{-/-} and *DKO* BM cells, while *Tet2* mRNA expression was not detectable in the *Tet2*^{-/-} and *DKO* BM cells, confirming the complete deletion of *Tet1* and/or *Tet2* transcripts in these mice (Figure S1A). This analysis also confirmed that there was no compensatory up-regulation of other *Tet* family genes in *Tet1*^{-/-}, *Tet2*^{-/-} and *DKO* BM cells (Figure S1A). Dot blot assays showed a significant reduction in 5hmC levels in *Tet1*^{-/-} and *Tet2*^{-/-} BM cells compared to WT BM cells (Figure S1B,C). A much lower 5hmC level was documented in *DKO* BM cells than in single knockout BM (Figure S1B,C). All mice in the study were maintained in a mixed 129 and C57BL/6 background. Animal care was in accordance with institutional guidelines, and approved by the Institutional Animal Care and Use Committee (IACUC), University of Miami Miller School of Medicine and Department of Comparative Medicine, Massachusetts Institute of Technology.

Real time PCR Analysis. Total RNA was isolated from B-ALL patient MNCs, healthy control

CD19⁺ cells, and BM cells of each mouse genotype and was treated with RNase-free DNase to remove contaminating genomic DNA. First-strand cDNA was synthesized. Real time PCR was performed using Fast SYBR Green master mix. PCR amplifications were performed in triplicate for each gene of interest along with parallel measurements of human *GAPDH* or mouse *β-actin* cDNA (internal controls). To confirm specific amplification of the desired PCR product, melting curves were analyzed and PCR products were separated on a 3% agarose gel. The primers for the mouse *Tet* and *Actin* are shown in our previous report (Li et al., 2011). The primers used for human *TET1* and *TET2* qPCR are as the following: TET1-5, 5'-AATGGAAGCACTGTGGTTTG-3'; TET1-3, 5'-ACATGGAGCTGCTCATCTTG-3'; TET2-5, 5'-GGCTACAAAGCTCCAGAATGG-3'; TET2-3, 5'-AAGAGTGCCACTTGGTGTCTC-3'.

Analysis of 5hmC levels using dot blot. Levels of 5hmC in BM cells were detected using dot blot as described previously (Ko et al., 2010). Genomic DNA was isolated from BM cells of WT, *Tet2*^{+/-}, *Tet2*^{-/-} or *DKO* mice. DNA samples were denatured and two-fold serial dilutions were spotted on nitrocellulose membranes. The blotted membranes were washed, air-dried, vacuum-baked, blocked and incubated with anti-5hmC antibody (1:1,000) overnight at 4°C. After incubating with secondary antibody, the membranes were visualized by enhanced chemiluminescence. Signal density was then quantified using FluorChem® HD2 (Alpha Innotech). To ensure equal spotting of total DNA on the membranes, the same blot was stained with 0.02% methylene blue in 0.3 M sodium acetate.

Analyses of mice. PB was collected by retro-orbital bleeding of mice and was smeared for May-Grunwald-Giemsa staining, and/or subjected to an automated blood count (Hemavet System 950FS). Morphological evaluation of BM and spleen samples were performed on cytopins (5×10⁵ cells/sample) followed by May-Grunwald-Giemsa staining. For histopathology analyses, femurs were fixed in formaldehyde, decalcified, and paraffin embedded. Spleens, livers, lymph nodes, kidneys and lungs were treated similarly except for the decalcification step.

Sections (4.5 μ m) were stained with hematoxylin/eosin (H&E) or antibody against B220 or CD43.

Constructs and transduction. The mammalian codon-optimized mouse DNA sequences of both WT Flag-Tet1 and mutant Flag-Tet1 (mTet1, H1620YxD1622A, catalytic activity inactive) were synthesized by SynBio Corp. and then ligated into a *pCDF1-IRES-GFP* lentiviral vector. MEL cells and *DKO* LSK cells were transduced with lentivirus encoding GFP, Tet1/GFP or mTet1/GFP as previously described (Copley et al., 2013). Western blot was performed with anti-Flag antibody to confirm the expression of Flag-Tet1 using GFP⁺ MEL cells. GFP⁺ LSK cells were sorted for re-plating assays.

Flow cytometry analysis, cell sorting, and hematopoietic progenitor cell (HPC) assay. Total PB white blood cells were obtained after lysis of red blood cells. Single-cell suspensions from BM, spleen, liver, and PB were stained with panels of fluorochrome-conjugated antibodies. Flow cytometric analysis of HSCs, HPCs, CLPs and BLPs were performed as previously described (Kondo et al., 1997; Niebuhr et al., 2013). Dead cells were excluded by DAPI staining. The analyses were performed using a BD FACSCantoII or LSRII flow cytometer. All data were analyzed by FlowJo7.6 software. For Lin⁻Sca-1⁺c-Kit⁺ (LSK) and GFP⁺ cell purification, FACS cell sorting was applied. For colony-forming unit (CFU) assays, BM (5×10^3 cells/plate) or spleen cells (5×10^4 cells/plate) were plated in triplicate in methylcellulose medium (Methocult M3231) supplemented with mIL-3 (10ng/mL), hIL-6 (100ng/mL), hEpo (4U/mL) and mSCF (100ng/mL), and scored in 8-10 days. For pre-B colonies, 10 ng/ml mIL-7 was used, and B-cell colonies were counted in 12-14 days.

Clonality Analysis. Genomic DNA was isolated from splenic B220⁺ cells of WT and *DKO* mice. Clonal rearrangement of IgH segment was amplified by PCR using the following primers: DSF-5, 5'-AGGGATCCTTGTGAAGGGATCTACTACTGTG-3'; JH4, 5'-AAAGACCTGCAGAGGCCATTCTTACC-3'. PCR products were separated by

electrophoresis through a 1.2% agarose gel and stained with ethidium bromide.

Tumor Transfer assay and competitive repopulation assay. The transplantability of B-cell malignancy was determined by injecting 1×10^6 spleen cells from the moribund *DKO* or WT mice into sublethally irradiated (600 cGy) C57BL/6 recipient mice (CD45.1, n=6) through tail veins (Figure S3A). Recipient mice were sacrificed when they became moribund or at 4 months after injection. The mice were analyzed to determine their hematological phenotype and development of B-cell malignancy. Donor cell chimeras in the PB, spleen and BM were examined at the end of the observation period. The competitive repopulation assay was performed by transplanting BM cells (1×10^6 , CD45.2⁺) from *Tet1^{fl/fl};Tet2^{fl/fl}*, *Tet2^{fl/fl};MxCre* or *Tet1^{fl/fl};Tet2^{fl/fl};MxCre* mice plus the competitor BM cells (1×10^6 , CD45.1⁺) from B6.SJL mice, into lethally irradiated (700 + 400 cGy) F1 mice (CD45.1/CD45.2) by tail vein injection (Figure 5A). Four weeks after transplantation, the recipient mice were assessed for CD45.2/CD45.1 chimeras in their PB by FACS analysis and then were induced for *Tet2* or *Tet1/2* deletion by three doses of *pI:pC* injections (300 µg, every other day). The contribution of CD45.1⁺ vs. CD45.2⁺ cells in the PB was monitored every 4-weeks for 28 weeks after *pI:pC* injections.

Genome-wide 5hmC Profiling (hME-Seal). hME-Seal was described previously (Song et al., 2011). Briefly, Genomic DNA was first sonicated to 100-500bp, and mixed with 100 µl solution containing 50mM HEPES buffer (pH 7.9), 25mM MgCl₂, 250mM UDP-6-N₃-Glu and 2.25mM wild-type β-glucosyltransferase. Reactions were incubated for 1h at 37°C. DNA substrates were purified via Qiagen DNA purification kit. 150mM dibenzocyclooctyne modified biotin was then added to the purified DNA, and the labeling reaction was performed for 2h at 37°C. The biotin-labeled DNA was enriched by Streptavidin-coupled Dynabeads (Dynabeads MyOne™ Streptavidin T1, Life Technologies) and purified by Qiagen DNA purification kit for library preparation.

Methylated DNA immunoprecipitation (MeDIP). MeDIP experiments were performed

according to the manufacturer's protocol (Active Motif). The enriched methylated DNA was purified by Qiagen DNA purification kit for library preparation.

Library preparation and high-throughput sequencing. Enriched DNA from MeDIP and hME-seal were subjected to library construction using the NEBNext ChIP-Seq Library Prep Reagent Set for Illumina according to the manufacturer's protocol. In brief, 25ng of input genomic DNA or experimental enriched DNA were utilized for each library construction. 150-300 bp DNA fragments were selected by AMPure XP Beads (Beckman Coulter) after the adapter ligation. An Agilent 2100 BioAnalyzer was used to quantify the amplified DNA, qPCR was applied to accurately quantify the library concentration. 20pM diluted libraries were used for sequencing. 50-cycle single-end sequencing was performed using Illumina HiSeq 2000. Image processing and sequence extraction were done using the standard Illumina Pipeline.

RNA-seq libraries were generated from duplicated samples per condition using the Illumina TruSeq RNA Sample Preparation Kit v2 following manufacturer's protocol. The RNA-seq libraries were sequenced as 50-cycle pair-end runs using Illumina HiSeq 2000.

Bioinformatics and statistical analyses. Bioinformatics analysis for 5hmC-seq and MeDIP-seq were described previously (Szulwach et al., 2011; Yao et al., 2014). Briefly, FASTQ sequence files were aligned to mm9 reference genome using Bowtie (Langmead et al., 2009). Peaks were identified by Model-based Analysis of ChIP-Seq (MACS) software (Zhang et al., 2008). Unique ChIP-seq, 5hmC-seq and MeDIP-seq mapped reads were plotted to various genomic regions by ngsplot (Shen et al., 2014) or R (<http://www.r-project.org/>). Annotation analyses were performed by HOMER (Heinz et al., 2010). Gene Ontology analysis was performed using DAVID (the database for annotation, visualization and integrated discovery) bioinformatics resources (Huang et al., 2009). RNA-seq reads were aligned using tophat v2.0.8 and differential RPKM expression values were extracted using cuffdiff v2.2.1 (Trapnell et al., 2009).

References:

- Copley, M.R., Babovic, S., Benz, C., Knapp, D.J., Beer, P.A., Kent, D.G., Wohrer, S., Treloar, D.Q., Day, C., Rowe, K., *et al.* (2013). The Lin28b-let-7-Hmga2 axis determines the higher self-renewal potential of fetal haematopoietic stem cells. *Nature cell biology* 15, 916-925.
- Dawlaty, M.M., Breiling, A., Le, T., Raddatz, G., Barrasa, M.I., Cheng, A.W., Gao, Q., Powell, B.E., Li, Z., Xu, M., *et al.* (2013). Combined deficiency of tet1 and tet2 causes epigenetic abnormalities but is compatible with postnatal development. *Developmental cell* 24, 310-323.
- Dawlaty, M.M., Ganz, K., Powell, B.E., Hu, Y.C., Markoulaki, S., Cheng, A.W., Gao, Q., Kim, J., Choi, S.W., Page, D.C., *et al.* (2011). Tet1 is dispensable for maintaining pluripotency and its loss is compatible with embryonic and postnatal development. *Cell stem cell* 9, 166-175.
- Heinz, S., Benner, C., Spann, N., Bertolino, E., Lin, Y.C., Laslo, P., Cheng, J.X., Murre, C., Singh, H., and Glass, C.K. (2010). Simple combinations of lineage-determining transcription factors prime cis-regulatory elements required for macrophage and B cell identities. *Molecular cell* 38, 576-589.
- Huang da, W., Sherman, B.T., and Lempicki, R.A. (2009). Systematic and integrative analysis of large gene lists using DAVID bioinformatics resources. *Nature protocols* 4, 44-57.
- Ko, M., Huang, Y., Jankowska, A.M., Pape, U.J., Tahiliani, M., Bandukwala, H.S., An, J., Lamperti, E.D., Koh, K.P., Ganetzky, R., *et al.* (2010). Impaired hydroxylation of 5-methylcytosine in myeloid cancers with mutant TET2. *Nature* 468, 839-843.
- Kondo, M., Weissman, I.L., and Akashi, K. (1997). Identification of clonogenic common lymphoid progenitors in mouse bone marrow. *Cell* 91, 661-672.
- Langmead, B., Trapnell, C., Pop, M., and Salzberg, S.L. (2009). Ultrafast and memory-efficient alignment of short DNA sequences to the human genome. *Genome Biol* 10, R25.
- Li, Z., Cai, X., Cai, C.L., Wang, J., Zhang, W., Petersen, B.E., Yang, F.C., and Xu, M. (2011). Deletion of Tet2 in mice leads to dysregulated hematopoietic stem cells and subsequent development of myeloid malignancies. *Blood* 118, 4509-4518.
- Niebuhr, B., Kriebitzsch, N., Fischer, M., Behrens, K., Gunther, T., Alawi, M., Bergholz, U.,

Muller, U., Roscher, S., Ziegler, M., *et al.* (2013). Runx1 is essential at two stages of early murine B-cell development. *Blood* 122, 413-423.

Shen, L., Shao, N., Liu, X., and Nestler, E. (2014). ngs.plot: Quick mining and visualization of next-generation sequencing data by integrating genomic databases. *BMC genomics* 15, 284.

Song, C.X., Szulwach, K.E., Fu, Y., Dai, Q., Yi, C., Li, X., Li, Y., Chen, C.H., Zhang, W., Jian, X., *et al.* (2011). Selective chemical labeling reveals the genome-wide distribution of 5-hydroxymethylcytosine. *Nature biotechnology* 29, 68-72.

Szulwach, K.E., Li, X., Li, Y., Song, C.X., Wu, H., Dai, Q., Irier, H., Upadhyay, A.K., Gearing, M., Levey, A.I., *et al.* (2011). 5-hmC-mediated epigenetic dynamics during postnatal neurodevelopment and aging. *Nature neuroscience* 14, 1607-1616.

Trapnell, C., Pachter, L., and Salzberg, S.L. (2009). TopHat: discovering splice junctions with RNA-Seq. *Bioinformatics* 25, 1105-1111.

Yao, B., Lin, L., Street, R.C., Zalewski, Z.A., Galloway, J.N., Wu, H., Nelson, D.L., and Jin, P. (2014). Genome-wide alteration of 5-hydroxymethylcytosine in a mouse model of fragile X-associated tremor/ataxia syndrome. *Human molecular genetics* 23, 1095-1107.

Zhang, Y., Liu, T., Meyer, C.A., Eeckhoute, J., Johnson, D.S., Bernstein, B.E., Nusbaum, C., Myers, R.M., Brown, M., Li, W., *et al.* (2008). Model-based analysis of ChIP-Seq (MACS). *Genome Biol* 9, R137.

Supplemental Figure legends:

Figure S1: Unlike *Tet2*^{-/-} mice, *Tet1/2* DKO mice do not display a CMML phenotype early in life, related to Figure 2. A cohort of WT (n=15), *Tet1*^{-/-} (n=14), *Tet2*^{-/-} (n=16), and DKO (n=12) mice were sacrificed at 3-4 months of age and hematological parameters were examined. **(A)** Quantitative RT-PCR analysis of *Tet1*, *Tet2*, and *Tet3* mRNA expression in BM cells from 5-7 week-old WT, *Tet1*^{-/-}, *Tet2*^{-/-} and DKO mice (4 mice/genotype). The relative mRNA expression of each *Tet* gene was determined using β -actin as internal calibrator. The mRNA expression levels are reported as relative expression units to the respective *Tet* expression in WT mice. **(B, C)** Genomic DNA was extracted from BM cells of 5-7 week-old WT, *Tet1*^{-/-}, *Tet2*^{-/-} and DKO mice and blotted onto nitrocellulose membrane after 2-fold serial dilution. 5hmC levels were detected with an anti-5hmC antibody. Methylene blue staining was performed to ensure equal spotting of total DNA on the membranes (B). Quantification of the signal density was shown (C). Representative data from 3 sets of animals is shown. **(D)** DKO mice exhibited normal blood counts in their PB at 3-4 months of age. There were no significant differences in each of the parameters of total blood counts (WBC, neutrophil, monocyte, lymphocyte, and RBC) between young *Tet1*^{-/-}, DKO and WT groups of mice. Consistent with our previous report (Li et al., 2011), the majority of the 3-4 month old *Tet2*^{-/-} mice exhibited increased WBC counts (accompanied by monocytosis and/or neutrophilia), moderately decreased red blood cell counts, and normal lymphocyte counts as compared to WT controls. **(E)** Unlike *Tet2*^{-/-} mice, DKO mice did not have splenomegaly at 3-4 months of age. Spleen weights of each genotype of mice (6-8 mice/genotype) were shown. Young *Tet1*^{-/-} and DKO mice had comparable spleen and liver size compared to WT controls, while *Tet2*^{-/-} mice clearly had splenomegaly and moderately enlarged livers (data not shown). **(F)** Colony forming capacity of BM cells from each mouse genotype at 3-4 months of age. Representative data from 3 sets of animals is shown. There were no differences in the number of each type of myeloid colonies in the BM and spleen (data not shown) of *Tet1*^{-/-}, DKO and WT groups of mice. In contrast, a dramatic increase in the number of Colony forming unit-Granulocyte/Macrophage (CFU-GM), Burst-forming unit-erythroid

(BFU-E) and CFU-Mix was observed in the BM and spleen of the *Tet2*^{-/-} mice. Collectively, these data indicate that up to 4 months of age, *DKO* mice do not exhibit the signs of CMML development that the *Tet2*^{-/-} mice robustly display at this age. * *P*<0.05, ** *P*<0.01, *** *P*<0.001

Figure S2: Most of the *DKO* and *Tet1*^{+/-};*Tet2*^{-/-} mice developed lethal B-lymphoid malignancy, related to Figure 2. (A) The B220/FSC FACS plots on the PB, BM, and spleen of representative moribund *DKO* (#G2-53 and #G3-56) and age matched WT mice. (B) Flow cytometric analysis of cell surface markers (B220, IgM, CD43, CD19, CD71, TdT and CD5) on splenic B-cell populations of representative moribund *DKO* mice (#G3-53, blue; and #G2-53, red). (C) Flow cytometric analysis of the granulocytic/monocytic (Gr1/Mac1), erythroid (Ter119/CD71) and T-cell (CD4/CD8) lineages in the PB and BM of a representative moribund *DKO* mouse with B-cell malignancy (#G3-56) and an age-matched WT control mouse. The numbers indicate the percentage of cells in each cell population. (D) May-Giemsa–stained BM and SP cytopsin-preparations (bar: 20µm) from representative moribund *DKO* mice (#G3-53 and #G2-53) and age matched WT mice. (E) Kaplan-Meier survival curve of *Tet1*^{+/-};*Tet2*^{-/-} (n=15) compared to WT (n=25), *DKO* (n=19), and *Tet2*^{-/-} (n=20) mice up to 600 days of life. (F) Pie charts show the percentage of various spectra of hematological malignancies in aged *Tet1*^{+/-};*Tet2*^{-/-}, *Tet1*^{-/-}, *Tet2*^{-/-}, and *DKO* mice (9-20 months old).

Figure S3: The B-cell malignancy in *DKO* mice is transplantable to secondary recipients, related to Figure 3. (A) Tumor transfer schema. Spleen cells (1x10⁶) from a WT mouse or a *DKO* mouse with B-cell malignancy (#G2-53) were each injected into 6 sublethally irradiated (600cGy) CD45.1⁺ B6.SJL recipients. (B) WBC, lymphocyte and RBC counts in the PB of recipients transplanted with WT (n=6) or *DKO* (n=4) spleen cells. (C) Pale footpads, enlarged lymph nodes and spleen in a representative recipient receiving *DKO* spleen cells. (D) Flow cytometric analysis of B-cell surface markers (B220, IgM, CD43, CD5, and CD71) on BM and spleen B-cell populations of a representative recipient receiving *DKO* spleen cells. The numbers indicate the percentage of cells in each cell population. (E) May-Giemsa–stained BM and spleen

cell cytospin-preparations (Bar: 20 μ m) from a representative recipient receiving WT or *DKO* spleen cells.

Figure S4: Generation of *Tet2:flox* and *Tet1:flox* allele mice, related to Figure 5. (A) Targeting strategy for *Tet2:floxed* allele mice. Exon 11 was replaced by a *loxP-exon11-loxP-FRT-Neo-FRT* cassette after the recombination. Rectangular black bars indicate exons. E, *EcoRI*. (B) Southern blot of ES cell DNA digested with *EcoRI* and hybridized with a genomic fragment external to the 5' arm with WT band 13,363 bp and recombinant band 5,365 bp (left panel), and a probe external to the 3' arm displayed WT band 13,363 bp and recombinant band 7,219 bp (right panel). (C) Schematic of alleles and strategy to generate *Tet1* conditional ESCs and mice from our previously reported *Tet1^{+H}* mESCs. (D) Southern blot confirmation of deletion of selection cassette to generate *Tet1^{+F}* mESCs. (E) Representative PCR analyses of *MxCre*-mediated *Tet1* and/or *Tet2* deletion in PB cells from *Tet1^{ff}*, *Tet2^{ff}*, *Tet1^{ff};Tet2^{ff}*, *Tet1^{ff};MxCre*, *Tet2^{ff};MxCre*, and *Tet1^{ff};Tet2^{ff};MxCre* mice 4 weeks after *pI:pC* injection. The genotyping primers for *Tet1* will give rise to a WT *Tet1* allele band of 963 bp, *Tet1 flox* allele band of 1100 bp, and a 600 bp band after recombination. The genotyping primers for *Tet2* (Forward: 5'-CATAGAGCTGTGTGTCCTGTTGTC-3'; Reverse: 5'-GTGGAACATTACCTAAGCGAGAACC-3') will give rise to a WT *Tet2* allele band of 1112 bp, *Tet2 flox* allele band of 1383 bp, and a 454 bp band after recombination. Details on Southern blot probe and PCR genotyping information for *Tet1:flox* allele mice are reported previously in Dawlaty et al (2011).

Figure S5: The effect of *pI:pC*-induced *Tet1/2* deletion on HSC/HPC pools *in vivo* and the effect of *Tet1* catalytic activity on *Tet2*-deletion mediated HSC/HPC hyper-replating potential *in vitro*, related to Figure 4. *Tet1^{ff};Tet2^{ff}*, *Tet1^{ff};MxCre*, *Tet2^{ff};MxCre* and *Tet1^{ff};Tet2^{ff};MxCre* mice were injected with *pI:pC*; after 5-6 weeks the frequencies of LSK (Lin⁻Sca-1⁺C-Kit⁺), CMP (Lin⁻Sca-1⁻c-kit⁺CD34⁺CD16/32^{mid}), MEP (Lin⁻Sca-1⁻c-kit⁺CD34⁺CD16/32^{lo}) and GMP (Lin⁻Sca-1⁻c-kit⁺CD34⁺CD16/32^{hi}) cell populations

within their BM cells were examined by flow cytometry. **(A)** Flow cytometric analysis of Sca-1⁺C-Kit⁺ and Sca-1⁻C-Kit⁺ cell populations in the total BM cells of representative *Tet1^{fl/fl};Tet2^{fl/fl}*, *Tet1^{fl/fl};MxCre*, *Tet2^{fl/fl};MxCre* and *Tet1^{fl/fl};Tet2^{fl/fl};MxCre* mice. **(B)** Quantitation of the percent LSK cells in the total BM cells of each genotype of mice (mean \pm SD, 4-5 mice/genotype). **(C)** Flow cytometric analysis of GMP, CMP and MEP cell populations in the Lin⁻Sca-1⁻c-Kit⁺ gated cell population of representative *Tet1^{fl/fl};Tet2^{fl/fl}*, *Tet1^{fl/fl};MxCre*, *Tet2^{fl/fl};MxCre* and *Tet1^{fl/fl};Tet2^{fl/fl};MxCre* mice. **(D)** Quantitation of the percent GMP, MEP and CMP cells in the Lin⁻Sca-1⁻c-Kit⁺ progenitor cell population of each genotype of mice (mean \pm SD, 4-5 mice/genotype). **(E)** Western blot was performed with MEL cells transduced with lentivirus encoding empty vector, WT Tet1 (Flag-Tet1) or catalytic domain inactive mutant Tet1 (Flag-mTet1). **(F)** Colony-formation assays were performed with GFP⁺ LSK cells sorted from each transduction (empty vector, Flag-Tet1 or Flag-mTet1) in methylcellulose medium (1,000 cells/plate). Colonies were passaged every 7 days for 3 sequential plating (P1-4). Data is a representative of 2 independent experiments. These results show that re-introducing WT Tet1, but not Tet1 (mTet1) into *DKO* LSK cells significantly increased their replating potential. * $P < 0.05$, ** $P < 0.01$

Figure S6: DMRs/DhMRs associated with *Tet2*^{-/-} and *DKO* LK cells and their correlation with HSC/leukemogenesis-related genes, related to Figure 6. **(A)** Venn diagram shows a significant overlap between DMRs identified in *DKO* vs WT cells, and the DMRs identified in *Tet2*^{-/-} vs WT LK cells. **(B)** Venn diagram shows a lack of overlap between DhMRs and DMRs identified in *Tet2*^{-/-} vs WT LK cells. **(C)** Venn diagram shows the overlap between the HSC/leukemogenesis-related gene bodies with DhMRs identified between *Tet2*^{-/-} and WT LK cells. A significant 245 out of 654 HSC/leukemogenesis-related genes are overlapped with those DhMRs. **(D)** Venn diagram shows the overlap between the HSC/leukemogenesis-related gene bodies with DMRs identified between *DKO* and WT LK cells. A significant 184 out of 654 HSC/leukemogenesis-related genes are overlapped with those DMRs. **(E)** Venn diagram shows the overlap between the HSC/leukemogenesis-related gene bodies with DMRs identified

between *Tet2*^{-/-} and WT LK cells. A significant 332 out of 654 HSC/leukemogenesis-related genes are overlapped with those DMRs.

Table S1. Diagnosis and phenotypic characteristics of the hematological malignancies in 10 moribund/deceased *DKO* mice, related to Figure 2.

Table S2: Diagnosis and phenotypic characteristics of the hematological malignancies in 9 moribund/deceased *Tet1*^{+/-};*Tet2*^{-/-} mice, related to Figure 2.

Table S3: Altered gene expression in different mutant background determined by RNA-seq, related to Figures 6 and 7.

Table S4: Overlapping genes lists from RNA-seq and TET1/TET2 ChIP-seq data, related to Figure 7.

Table S5: List of DhMRs associated with the loss of Tet2, related to Figure 6.

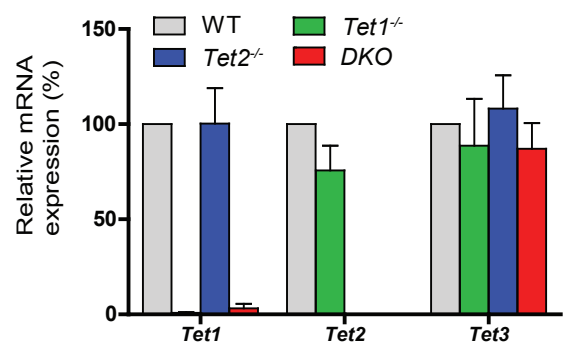
Table S6: List of DMRs associated with the loss of Tet2, related to Figure 6.

Table S7: List of DhMRs associated with the loss of Tet1 and Tet2, related to Figure 6.

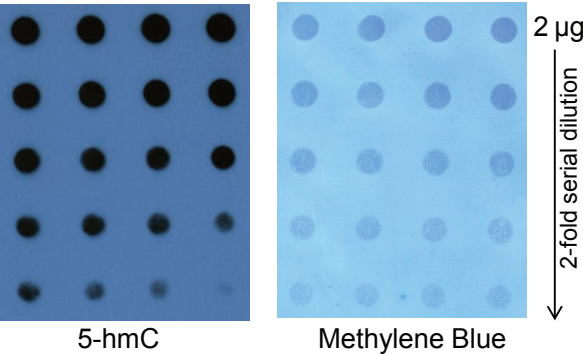
Table S8: List of DMRs associated with the loss of Tet1 and Tet2, related to Figure 6.

Figure S1

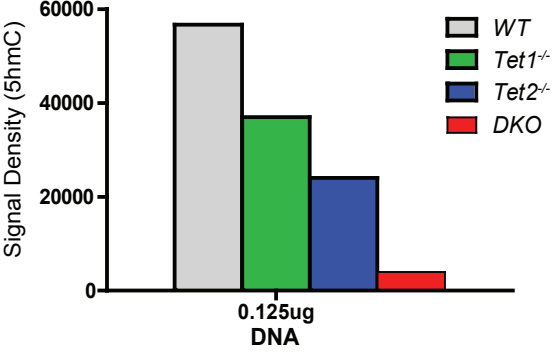
A



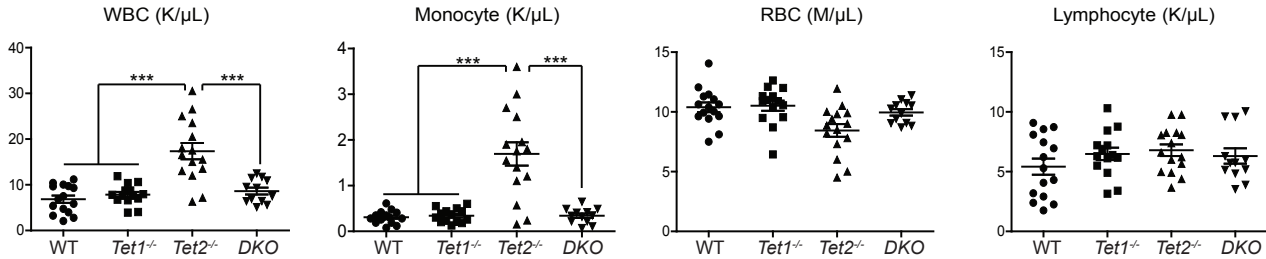
B



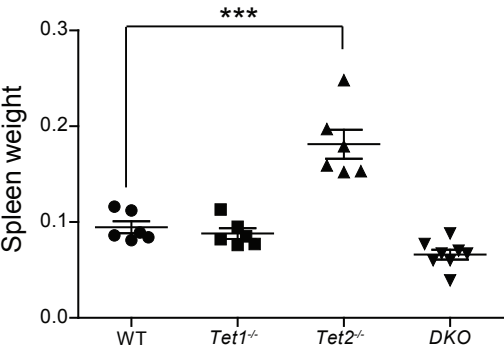
C



D



E



F

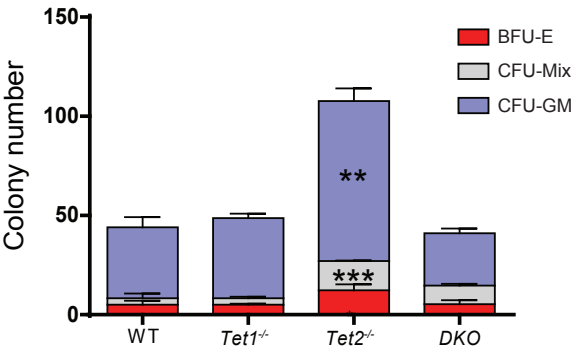


Figure S2

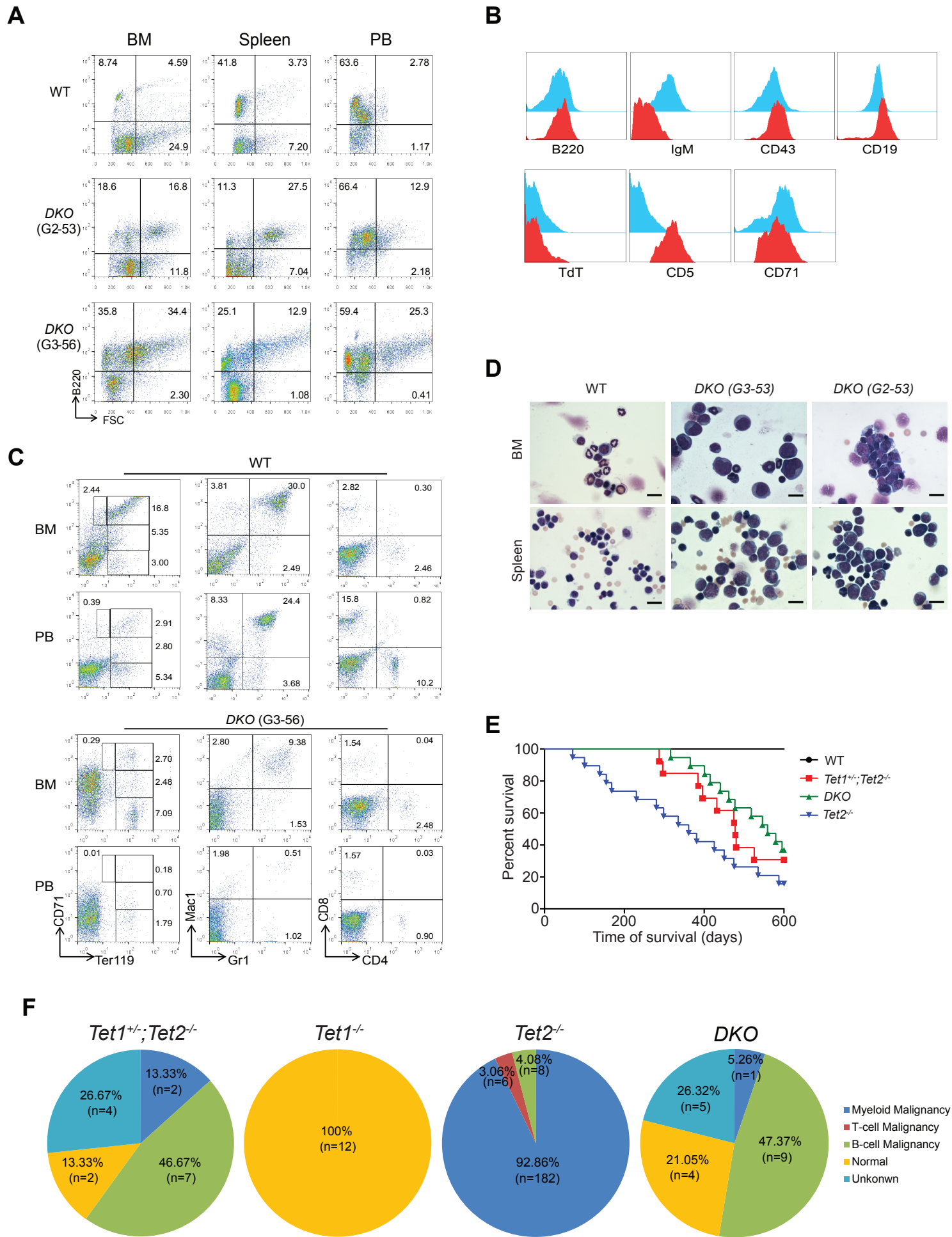


Figure S3

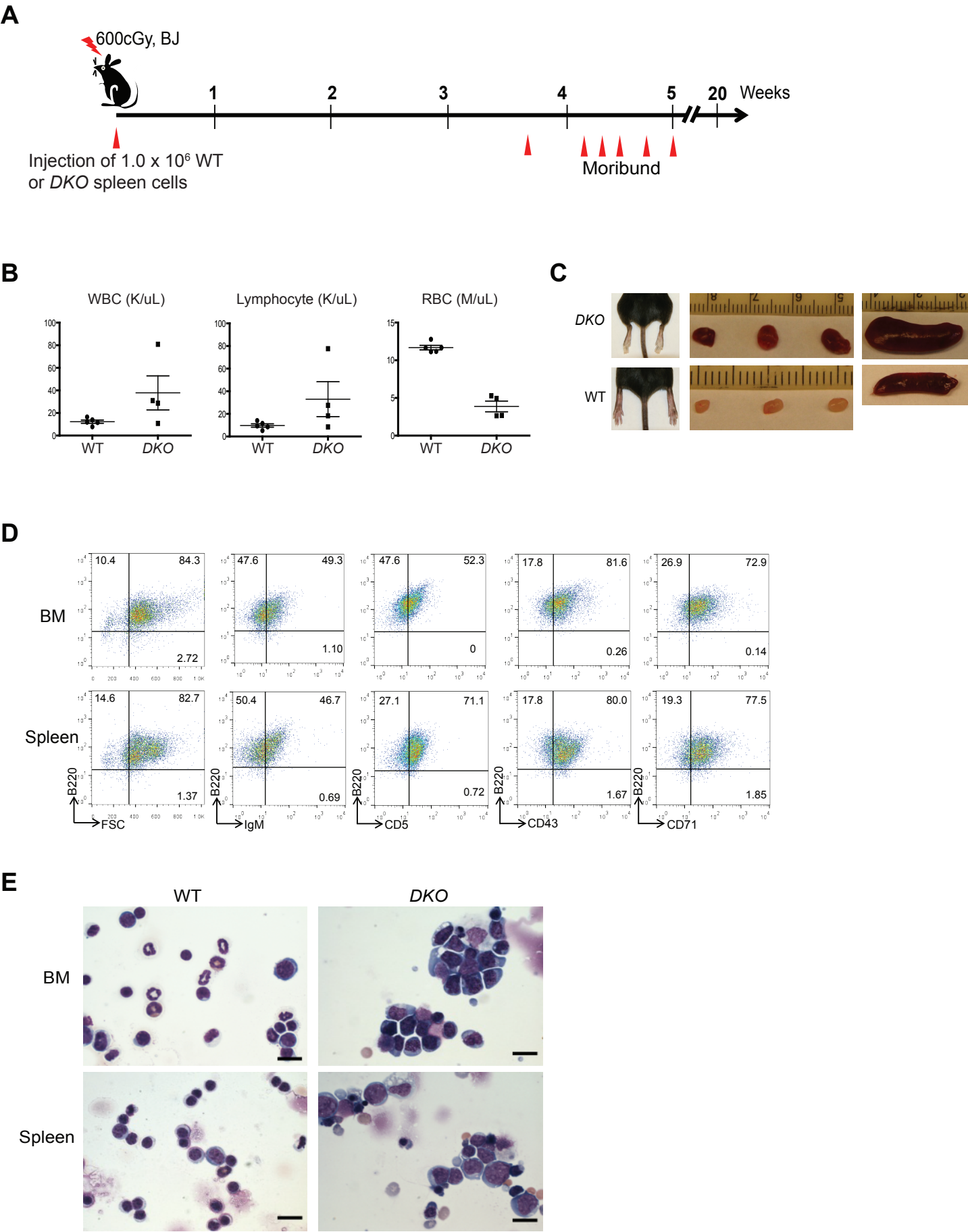


Figure S4

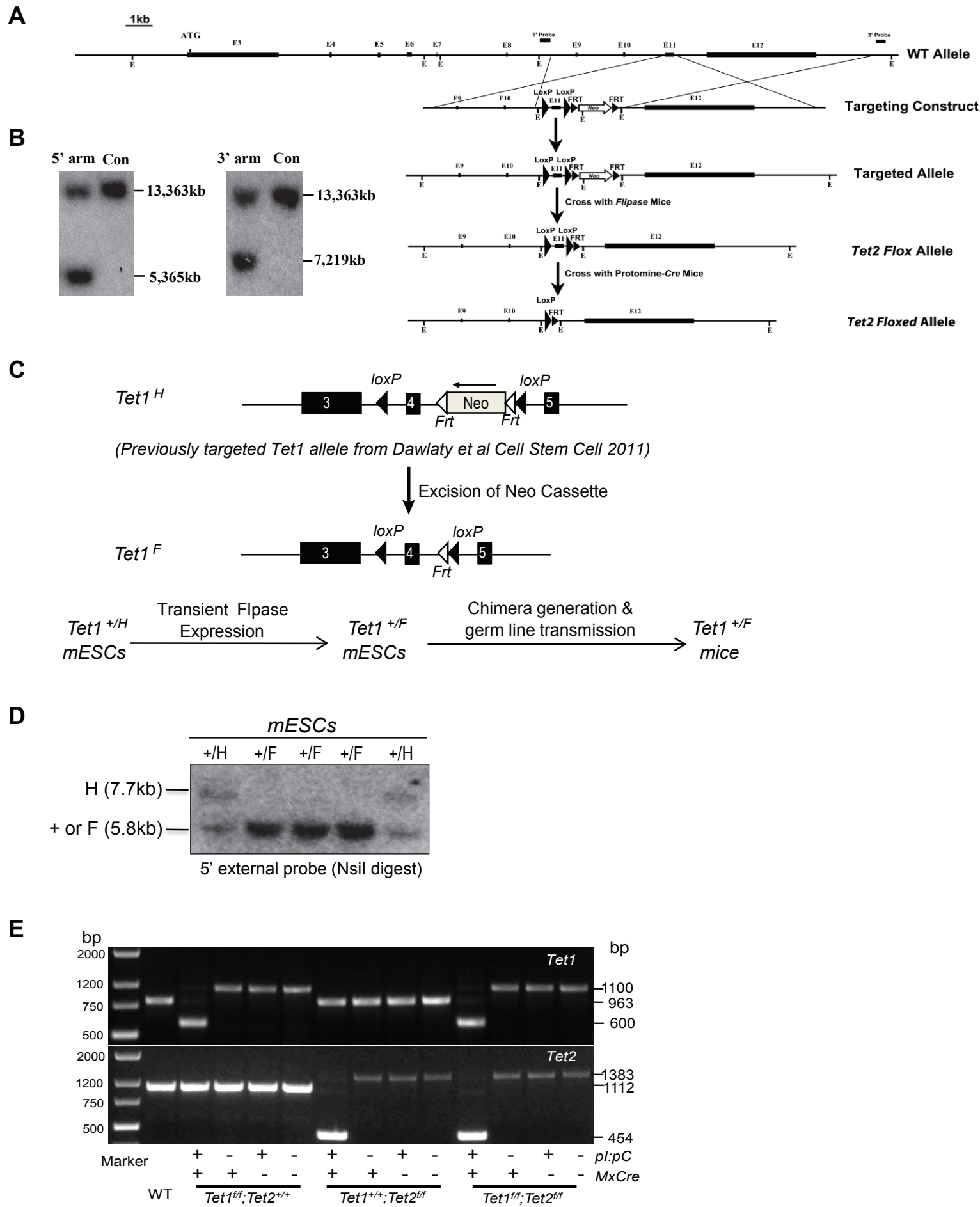


Figure S5

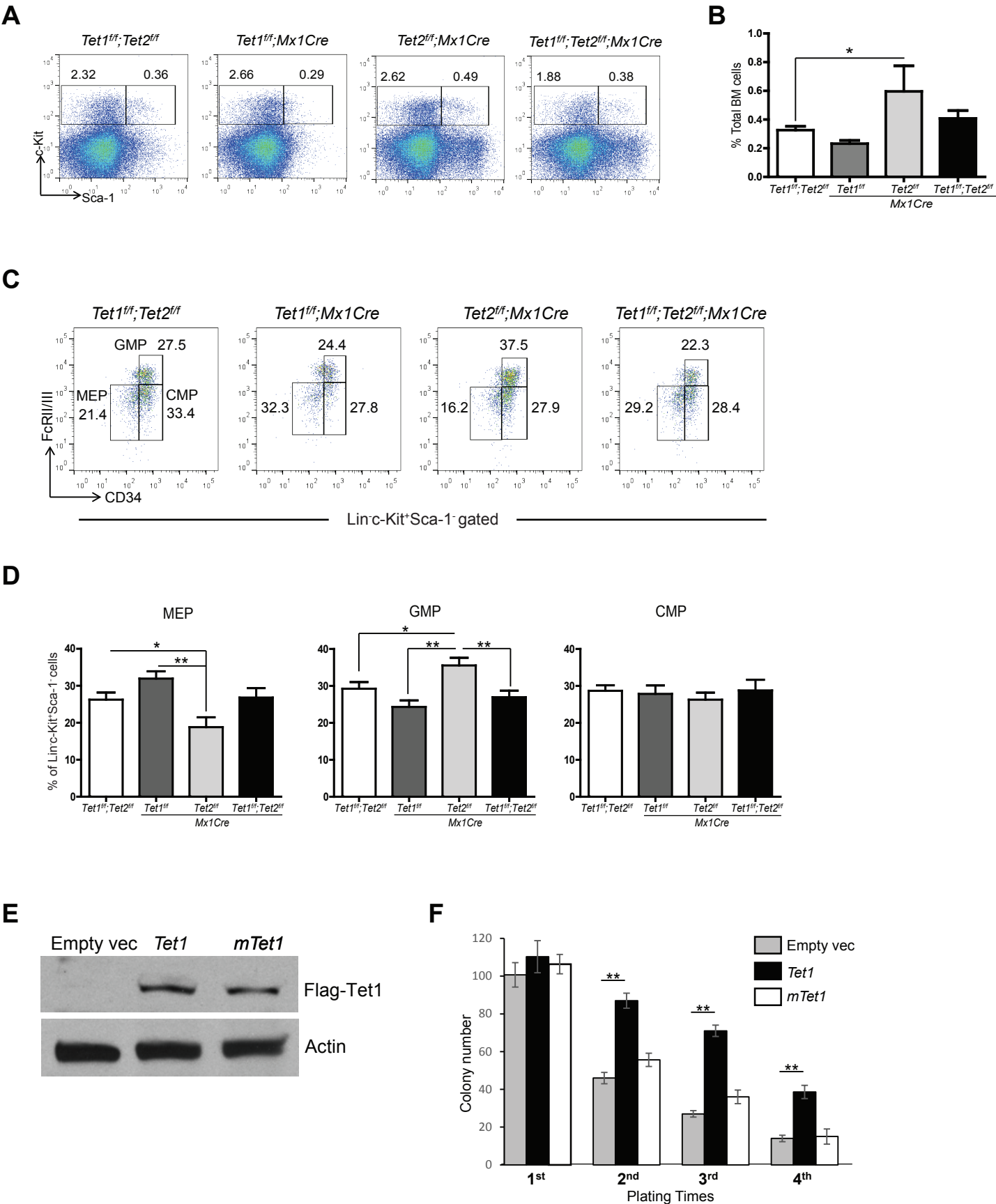


Figure S6

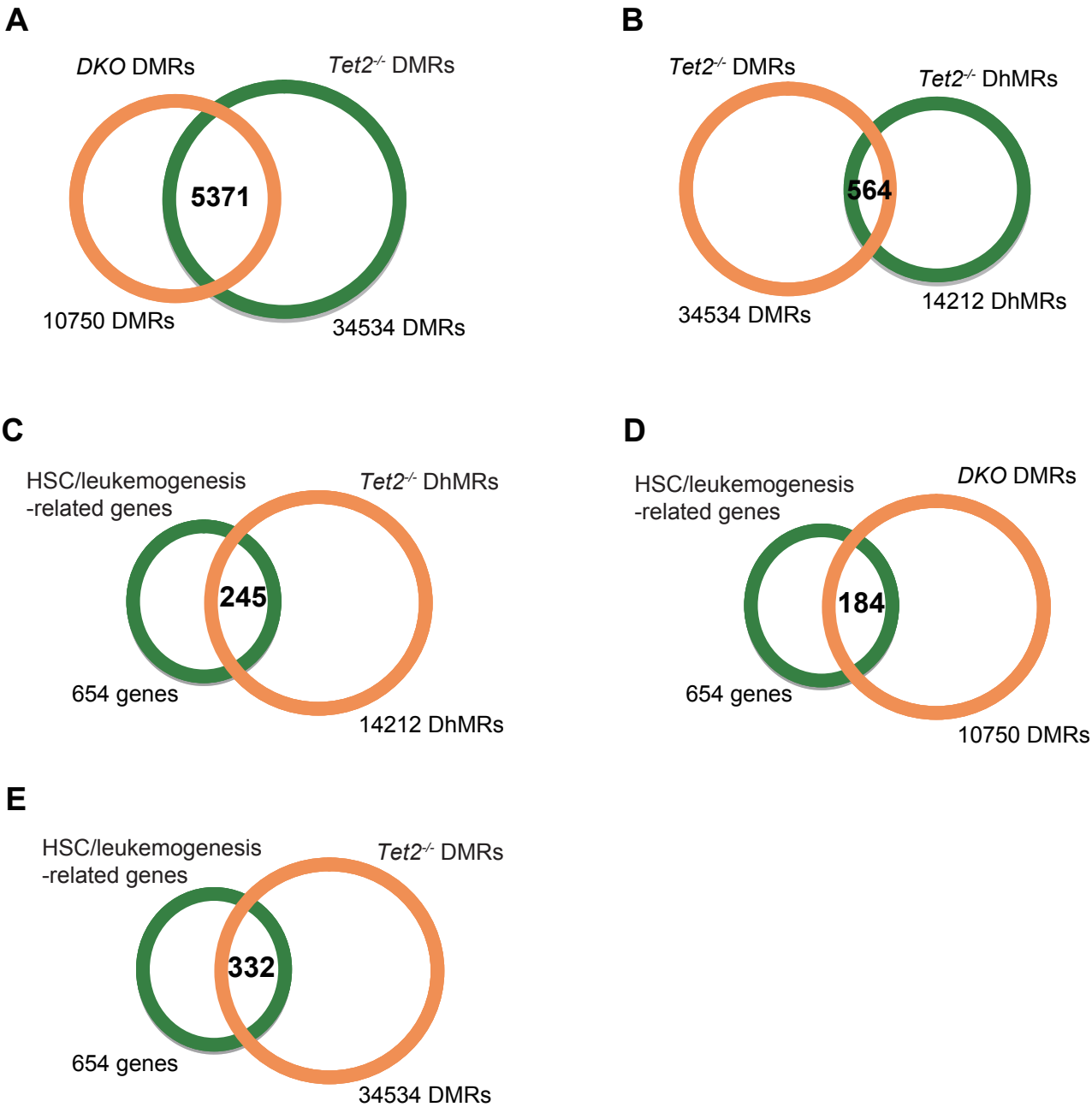


Table S1. Diagnosis and phenotypic characteristics of hematological malignancies in moribund/deceased *DKO* mice

ID	Age, (month)	Necropsy findings	Histology	Tumor Cell Marker	Blood Counts			IgH Rearrangement	Diagnosis
					WBC, K/ μ L	Ly, K/ μ L	RBC, M/ μ L		
G2-53	20	Hepatosplenomegaly, Lymphadenopathy	Invasion of bone marrow, spleen, liver, lymph nodes	B220 ⁺ IgM ^{lo/-} CD19 ⁺ CD43 ⁺ CD5 ⁺ TdT ⁺ IgD ⁺ IgE ⁺ IgG1 ⁺ IgG2a ⁺ b ⁻ Ig λ ⁺ Ig κ ⁺	88.8	85.7	9.32	Yes	B-ALL
G3-53	18	Hepatosplenomegaly, Lymphadenopathy	Invasion of bone marrow, spleen, liver, lymph nodes	B220 ⁺ IgM ⁺ CD19 ⁺ CD43 ⁺ CD5 ⁻ TdT ⁺ IgD ⁺ IgE ⁺ IgG1 ⁺ IgG2a ⁺ b ⁻ Ig λ ⁺ Ig κ ⁺	34.96	33.39	10.24	Yes	B-ALL
G3-81	15.5	Hepatosplenomegaly, Lymphadenopathy	Invasion of bone marrow, spleen, liver, lymph nodes	B220 ^{low} IgM ⁺ CD19 ⁺ CD43 ⁺ CD5 ⁻ TdT ⁺ IgD ⁺ IgE ⁺ IgG1 ⁺ IgG2a ⁺ b ⁻ Ig λ ⁺ Ig κ ⁺	42.34	41.49	8.55	Yes	B-ALL
G3-56	19.5	Hepatosplenomegaly, Lymphadenopathy	Invasion of bone marrow, spleen, liver, lymph nodes	B220 ⁺ IgM ^{lo/-} CD19 ⁺ CD43 ⁺ CD5 ⁺ TdT ⁺ IgD ⁺ IgE ⁺ IgG1 ⁺ IgG2a ⁺ b ⁻ Ig λ ⁺ Ig κ ⁻	77.54	74.61	1.16	Yes	B-ALL
G3-22	13	Hepatosplenomegaly	Invasion of bone marrow, spleen, liver	B220 ⁺ IgM ⁺ CD19 ⁺ CD43 ⁺ CD5 ⁺ TdT ⁺ IgD ⁺ IgE ⁺ IgG1 ⁺ IgG2a ⁺ b ⁻ Ig λ ⁺ Ig κ ⁺	16.72	14.4	11.19	Yes	B-ALL
G3-40	12.5	Hepatosplenomegaly, Lymphadenopathy	Invasion of bone marrow, spleen, liver, lymph nodes	B220 ⁺ IgM ⁺ CD19 ⁺ CD43 ⁺ CD5 ⁺ TdT ⁺ IgD ⁺ IgE ⁺ IgG1 ⁺ IgG2a ⁺ b ⁻ Ig λ ⁺ Ig κ ⁻	Very High	Very High	6.72	N/A	B-ALL
G3-63	13.5	Hepatosplenomegaly	Invasion of bone marrow, spleen, liver	B220 ⁺ IgM ⁺ CD19 ⁺ CD43 ⁺ TdT ⁻	13.40	10.47	10.44	N/A	B-ALL
G3-97	17.5	Hepatosplenomegaly, Lymphadenopathy	Invasion of bone marrow, spleen, liver, lymph nodes	B220 ⁺ IgM ⁺ CD19 ⁺ CD43 ⁺ CD5 ⁺ TdT ⁻	22.14	21.83	8.69	N/A	B-ALL
G3-15	9	Hepatosplenomegaly	Invasion of bone marrow, spleen, liver	B220 ⁺ IgM ⁺ CD19 ⁺ CD43 ⁺ TdT ⁻	20.66	17.12	9.1	N/A	B-ALL
G3-21	15	Hepatosplenomegaly	Invasion of spleen, liver	CD11b ⁺ F4/80 ⁺ Gr1 ^{lo}	50.2	7.53	6.76	No	CMML

Table S2. Diagnosis and phenotypic characteristics of hematological malignancies in 9 moribund/deceased *Tet1*^{+/-};*Tet2*^{-/-} mice

ID	Age (month)	Necropsy findings	Tumor Cell Marker	Blood Counts			Diagnosis
				WBC, K/ μ L	Ly, K/ μ L	RBC, M/ μ L	
G3-253	8.5	Hepatosplenomegaly, Lymphadenopathy	B220 ⁺ IgM ⁺ CD19 ⁺ CD43 ⁺ CD5 ⁺ TdT ⁻	46.3	42.4	10.75	B-ALL
G3-109	14	Hepatosplenomegaly	B220 ⁺ IgM ⁺ CD19 ⁺ CD43 ⁺ CD5 ⁺ TdT ⁻	12.1	9.2	8.7	B-ALL
G3-145	13.5	Hepatosplenomegaly, Lymphadenopathy	B220 ⁺ IgM ⁺ CD19 ⁺ CD43 ⁺ CD5 ⁺ TdT ⁻	38.6	35.5	10.53	B-ALL
G3-146	13.5	Hepatosplenomegaly, Lymphadenopathy	B220 ^{lo} IgM ⁺ CD19 ⁺ CD43 ⁺ TdT ⁻	74.4	71.2	8.48	B-ALL
G3-67	15	Hepatosplenomegaly	B220 ⁺ IgM ⁺ CD19 ⁺ CD43 ⁺ CD5 ⁺ TdT ⁻	36.9	34.1	9.19	B-ALL
G3-34	13	Hepatosplenomegaly, Lymphadenopathy	B220 ⁺ IgM ⁺ CD19 ⁺ CD43 ⁺ CD5 ⁺ TdT ⁻	18.2	10.3	10.26	B-ALL
G3-37	13	N/A	B220 ⁺ IgM ⁺	108.1	105.3	7.68	B-ALL
G2-142	12.5	Hepatosplenomegaly Pelvic myeloid sarcoma	CD11b ⁺ Gr1 ^{lo}	41.7	9.6	9.47	MPD-like myeloid leukemia
G3-28	15.5	Hepatosplenomegaly	CD11b ⁺ F4/80 ⁺ Gr1 ⁺	N/A	N/A	N/A	CMML